Hindawi
Shock and Vibration
Volume 2022, Article ID 3677691, 10 pages
https://doi.org/10.1155/2022/3677691

Research Article

Dynamic Characteristics of the Helical Planetary Transmission System considering the Installation Error of Shaft

Hongfei Zhai,[1,2] **Junjian Hou**,[1,2] **Zhanpeng Fang**,[1,2] **Yanqiu Xiao**,[1,2] **Lei Yao**,[1,2] **and Liangwen Wang**[1]

[1]*Mechanical and Electrical Engineering Institute, Zhengzhou University of Light Industry, Zhengzhou 450002, China*
[2]*Henan Engineering Research Center of New Energy Vehicle Lightweight Design and Manufacturing, Zhengzhou University of Light Industry, Zhengzhou 450002, China*

Correspondence should be addressed to Hongfei Zhai; hongfeizhai@zzuli.edu.cn

Received 22 October 2021; Accepted 20 May 2022; Published 6 July 2022

Academic Editor: Sandro Carbonari

The helical planetary transmission system (HPTS) is widely used in wind power, hydropower, and shield machine, which operating conditions are extremely complicated, and the existence of component installation errors will result in response deviations to the theoretical design. A dynamic model for slice type bending-torsional-pendulum of the HPTS is established in the lumped parameter method considering the installation error of shaft (IEOS) for the 1st planet gear, helical meshing characteristics, and bearing support characteristics. The vibration response characteristics of the HPTS under the IEOS for the 1st planet gear are studied. The results have shown that the FFT amplitudes for the horizontal vibration acceleration of the sun gear increased by 8.3%, and the axial vibration acceleration of the ring gear increased by 11.5%, respectively. The maximum magnitude increase of FFT amplitude for the vibration acceleration under a positive 0.13 mm IEOS for the 1st planet gear is the axial direction of the ring gear. The results indicate that the IEOS needs to be thoroughly introduced into the HPTS to simulate the actual operating conditions of the system.

1. Introduction

Based on the inevitably various errors that existed in the installation and debugging of mechanical parts, the existence of installation errors will cause deviations in the vibration, meshing force, and dynamic response characteristics of the gear transmission system, resulting in a linear decrease in system reliability and operational stability. The helical gear planetary transmission system is widely used in wind power generation, hydropower generation, and nuclear power generation. Its operating conditions are extremely complex, and the existence of component installation errors will produce response deviations to the theoretical design system, and its dynamic characteristics are economical and reliable for the whole machine. Sex and longevity have an important impact.

At present, many scholars investigated the component errors and response characteristics of the planetary gear transmission system. A dynamic model of wind turbine gearbox containing stiffness of bearing, stiffness of gear meshing, and flexibility of structure in multibody dynamic method was established by Helsen et al. [1, 2], and the dynamic responses of high-power wind turbine gearbox were studied. Zhao et al. [3] established a pure torsional dynamic model of wind turbine gearbox transmission, and the influences of transmission errors, input load, and mesh stiffness of gear pair on vibration responses of system components were studied. The effects of the position errors and eccentricity errors for planet gear on load characteristics and motion locus were researched by Velex et al. [4, 5].

A bending-torsional-pendular dynamic model of spur planetary transmission system considering the influences of the elastic deformation for ring gear, gyro effect, and centripetal acceleration was established by Wang et al. [6], the influence inherent characteristics of the system were analyzed, and the results showed that the nonstability of system parameters is determined by the multiscale method.

Tatar et al. [7] proposed a dynamic model of the planetary gear transmission system on the influences of the gyro effect and the rotating shaft. The studies show that the vibration modes of the helical planetary transmission system are divided into torsion-axial, lateral, and gearbox coupling. Shen et al. [8] built a pure torsional dynamic model of the planetary transmission system considering the wear of the tooth surface. The wear of the tooth surface is characterized by the static transmission error and time-varying mesh stiffness. The time-domain and frequency-domain response characteristics of the system vibration were analyzed. The results pointed out that the tooth surface wear will cause a significant difference between the time-domain and frequency-domain response of the system vibration.

Liu et al. [9] established a bending-torsional-pendular coupled dynamic model for herringbone tooth planetary transmission of wind turbine gearbox considering tooth separation and tooth profile error, and the influence of tooth error on mesh forces of gear pairs and vibration responses was studied. Mbarek et al. [10] analyzed the spectrum characteristics of the planetary transmission system under different loads and changes in the meshing stiffness of gear pair, and the results showed that the grid stiffness change has a certain degree of influence on the natural frequency of the system. A translational-torsional dynamic model of the planetary transmission system considering the time-varying transmission path factors was established by Zghal et al. [11]. The time-domain and frequency-domain responses of the system vibration were investigated, and the theoretical analysis results were verified with experiments.

Taheri et al. [12] presented a dynamic model of the planetary gear transmission system considering the deformation of the elastic ring gear and studied the meshing force response and vibration response characteristics of the system. The results showed that the meshing of gear pair has a strong influence on the system response. Park et al. [13] established a universal dynamic model of planetary gear transmission system considering the factors of the planet gear variability in transmission load and gear tooth deformation and studied the vibration response characteristics of the system under fault conditions.

Due to the comprehensive influences of the gear production technique, machining, installation, and debugging, manufacturing and installation errors exist in the gear transmission process. Therefore, the influences of the manufacturing and installation errors for the gear on the vibration characteristics of the HPTS must not be neglected. Kahraman et al. [14, 15] represented a manufacturing error, then the influence of random tooth pitch error on the vibration behavior of spur gear pairs was analyzed, and the effect of the gear roughness and rotational speed on the galling load was studied.

According to the bearing load characteristics and working conditions, Parker et al. [16, 17] established a dynamic model of the gear system considering the time-varying bearing support stiffness and studied the response characteristics of the system. Then, the vibration modal characteristics of the planetary gear transmission system containing an elastic body were investigated under the condition of the flexible ring gear. The results show that the elastic resonance phenomenon of the system will lead to fatigue or stress concentration in the core components of the transmission system.

Ren et al. [18] established a dynamic model of the herringbone planetary gear system considering the factors of the gear manufacturing error, time-varying meshing stiffness, and bearing deformation, focused on the gear tooth profile error and manufacturing eccentricity error, and studied the effect of the manufacturing error on the planetary transmission system. The results show that the manufacturing error has a great influence on the vibration characteristics of the system. Liu et al. [19] studied the changes in the pressure angle and overlap ratio for the sun gear during the floating process of the planetary transmission system and explored the phase modulation through the dynamic response of the system.

A lumped parameter dynamic model of a 5-slice type HPTS is established considering the factors of the IEOS for planetary gear and the time-varying meshing characteristics of gear pairs. Furthermore, the IEOS of the 1st planet gear was considered as the design variable. The effects of the IEOS on the system vibration characteristics were investigated.

2. Structure and Transmission Principle of HPTS

An HPTS is composed of 5 evenly distributed planet gears, carrier, ring gear, and sun gear as shown in Figure 1. The carrier of the HPTS is the input part, and the sun gear of the HPTS is the output part. The parameters for the HPTS are listed in Table 1.

The whole teeth of spur gear planetary transmission enter into meshing or exit meshing, which has a large meshing impact force. The gear meshing of the HPTS is an asymptotic meshing process along the space meshing contact line, causing the meshing contact is relatively stable. Meanwhile, due to the existence of a helix angle for the helical gear, the helical gear has transverse and overlap contact ratios, and the bearing capacity of the HPTS is relatively high. Therefore, the HPTS can effectively homogenize the impact load and reduce the impact of the load on the transmission system, which has good meshing stability, transmission stability, and large bearing capacity [20, 21].

The existence of the IEOS will lead to the instability of the actual operating characteristics of the HPTS, and even cause the system to fail to meet the design requirements and cause unexpected damage. Based on the meshing characteristics and conditions of the internal and external gear pairs of the HPTS considering the constituent factors and structural characteristics of the slice-type gears, each transmission component of the system is divided into five equal slices according to the material mechanics' relationship. The influence of directional stiffness and damping (horizontal direction, vertical direction, axial direction, and torsion direction) is shown in Figure 2.

Based on the ISO 1328-1-2013 cylindrical gear tooth surface deviation, ISO 6331 spur gear helical gear load capacity calculation, and GB/T 19073–2018 wind turbine

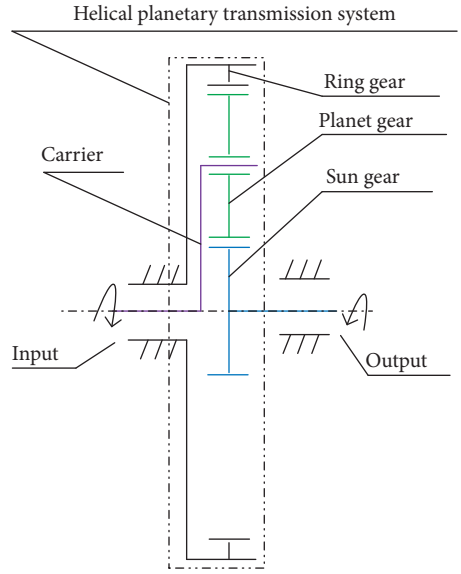

Figure 1: Structure and transmission principle of the HPTS.

Table 1: Gear parameters of the HPTS.

Gear date	Ring gear	Sun gear	Planet gear	Carrier
Number of teeth	91	29	31	—
Module (mm)	23	23	23	—
Pressure angle (°)	25	25	25	—
Helix angle (°)	5	5	5	—
Mass (Kg)	4400	1190	1070	7140
Moment of Inertia (N·m/rad)	5560	75.44	96.10	3730
Addendum coefficient		1		
Dedendum coefficient		1.5		

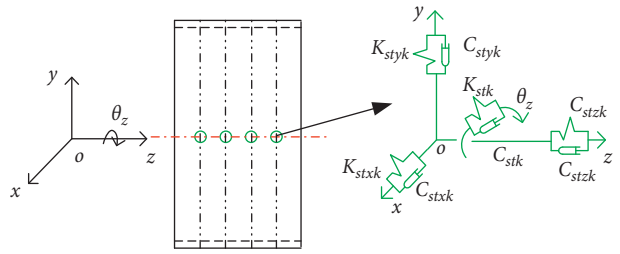

Figure 2: The mechanical model of a 5 equal slicing type gear.

gearbox design requirements, the influence of the IEOS on the meshing gear pair was considered to refer to the upper and lower deviation of the involute cylindrical gear axis angle. The axis angle deviation is set at 0.130 mm as shown in Figure 3. The K represents the connection stiffness of the component. The C characterizes the connection damping of the component. The subscript stxk (styk, stzk, stk) represents the kth position for the sun gear along the x (y, z, θ) direction.

Because each component of the helical planetary transmission system is divided into 5 equal slices, according to the meshing principle of the helical planetary transmission gear pair, the gear shaft installation error factor is considered, as shown in the following equation:

$$\Delta_{espi,erpi} = \pm K_i E_p, \tag{1}$$

where $\Delta_{espi,erpi}$ is the IEOS of the HPTS sun-planet (ring-planet) gear pair along the meshing line direction; Ki is the error ratio corresponding to the ith slice; Ep is the deviation of the IEOS.

According to the movement relationship and transmission characteristics of the transmission components, the helical gear meshing principle, and the bearing support

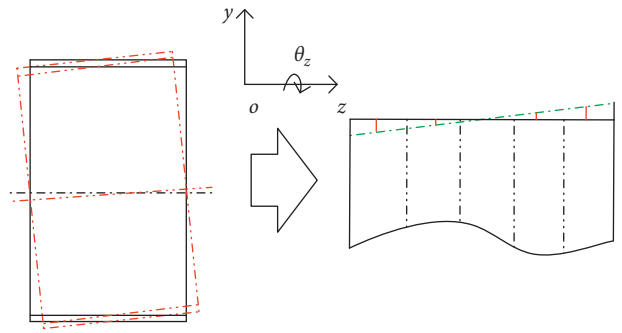

Figure 3: Influence of installation shaft error on helical gear meshing gear pair.

characteristics, the dynamic model of the slice type for the HPTS is established as shown in Figure 4.

Each transmission of the system is considered as a rigid body with 4 degrees of freedom (horizontal x, vertical y, axial z, and torsion θ). The center of the sun gear is set as the static coordinate origin, and the sun gear, planetary gear, and ring gear are set as static coordinate systems, respectively. The 5 moving coordinate systems are set as the each planet gear (u, v, w) correspondingly and the center of the each planet gear is set as the moving coordinate origin. The z-axis counterclockwise is set as positive. The subscripts s, c, r, and pi represent the sun gear, planet carrier, ring gear, and the ith planet gear. The K represents the spring stiffness of the components. The C characterizes the damping of the components. The subscript spi (rpi) represents the gear meshing of the ith sun-planet (ring-planet) gear pair.

The total transmission errors of the SP and RP meshing gear pairs for the HPTS along the meshing line considering the influence of the IEOS are as follows:

Sun-planet ring-planet

$$\Delta_{spi,rpi} = \delta_{spi,rpi} + E_{spi,rpi} \pm \Delta_{espi,erpi}, \tag{2}$$

where $\Delta_{spi,rpi}$ is the total transmission error of the sun-planet (ring-planet) gear pair; $\delta_{spi,rpi}$ is the static transmission error of the sun-planet (ring-planet) gear pair.

According to the Lagrange energy method, the motion equation of the 5-slice type helical planetary transmission system can be obtained as follows:

Kinetic equations of the 1st stage sun gear

$$\begin{aligned}
&\sum_{j=1}^{5} I_{sj}\ddot{\theta}_{sj} + \sum_{j=1}^{5} C_{s\theta j}\dot{\theta}_{sj} + \sum_{k=1}^{4} C_{stk}\left(\dot{\theta}_{sk} - \dot{\theta}_{s(k+1)}\right) + \sum_{j=1}^{5}\sum_{i=1}^{N} C_{spij}(t)\frac{\partial \Delta_{spij}}{\partial \theta_{sj}}\cos\beta_b \\
&+ \sum_{j=1}^{5} K_{s\theta j}\theta_{sj} + \sum_{k=1}^{4} K_{stk}\left(\dot{\theta}_{sk} - \dot{\theta}_{s(k+1)}\right) + \sum_{j=1}^{5}\sum_{i=1}^{N} K_{spij}(t)\Delta_{spi}\cos\beta_b = T_{out}, \\
&\cdot \sum_{j=1}^{5} m_{sj}\ddot{x}_{sj} + \sum_{j=1}^{5} C_{sxj}\dot{x}_{sxj} + \sum_{k=1}^{4} C_{stxk}\left(\dot{x}_{sk} - \dot{x}_{s(k+1)}\right) + \sum_{j=1}^{5}\sum_{i=1}^{N} C_{spij}(t)\frac{\partial \Delta_{spij}}{\partial x_{sj}}\sin\left(\varphi_i + \alpha_{sp}\right)\cos\beta_b \\
&+ \sum_{j=1}^{5} K_{sxj}x_{sxj} + \sum_{k=1}^{4} K_{stxk}\left(x_{sk} - x_{s(k+1)}\right) + \sum_{j=1}^{5}\sum_{i=1}^{N} K_{spij}(t)\Delta_{spij}\sin\left(\varphi_i + \alpha_{sp}\right)\cos\beta_b = 0, \\
&\cdot \sum_{j=1}^{5} m_{sj}\ddot{y}_{sj} + \sum_{j=1}^{5} C_{syj}\dot{y}_{sj} + \sum_{k=1}^{4} C_{styk}\left(\dot{y}_{sk} - \dot{y}_{s(k+1)}\right) - \sum_{j=1}^{5}\sum_{i=1}^{N} C_{spij}(t)\frac{\partial \Delta_{spij}}{\partial y_{sj}}\cos\left(\varphi_i + \alpha_{sp}\right)\cos\beta_b \\
&+ \sum_{j=1}^{5} K_{syj}y_{sj} + \sum_{k=1}^{4} K_{styk}\left(y_{sk} - y_{s(k+1)}\right) - \sum_{j=1}^{5}\sum_{i=1}^{N} K_{spi}(t)\Delta_{spi}\cos\left(\varphi_i + \alpha_{sp}\right)\cos\beta_b = 0, \\
&\cdot \sum_{j=1}^{5} m_{sj}\ddot{z}_{sj} + \sum_{j=1}^{5} C_{szj}\dot{z}_{sj} + \sum_{k=1}^{4} C_{stzk}\left(\dot{z}_{sk} - \dot{z}_{s(k+1)}\right) + \sum_{j=1}^{5}\sum_{i=1}^{N} C_{spij}(t)\frac{\partial \Delta_{spij}}{\partial z_{sj}}\sin\beta_b \\
&+ \sum_{j=1}^{5} K_{szj}z_{sj} + \sum_{k=1}^{4} K_{stzk}\left(z_{sk} - z_{s(k+1)}\right) + \sum_{j=1}^{5}\sum_{i=1}^{N} K_{spij}(t)\Delta_{spij}\sin\beta_b = 0.
\end{aligned} \tag{3}$$

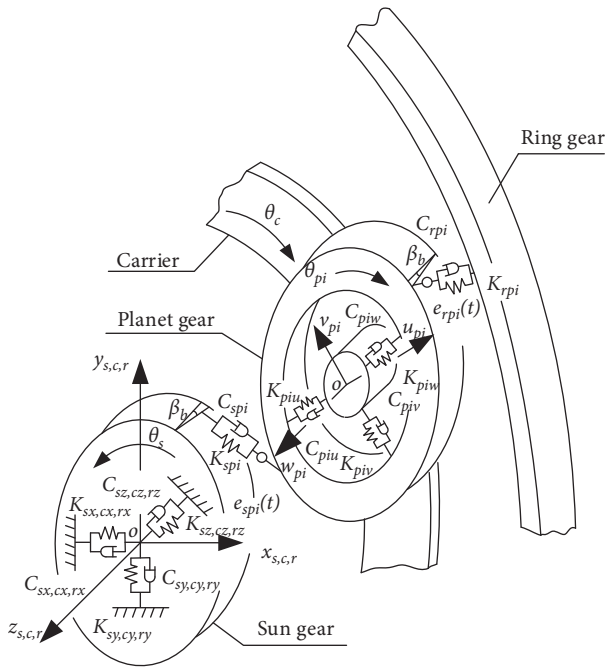

Figure 4: Dynamic model of slice type HPTS.

Kinetic equations of the 1st stage ring gear

$$
\begin{aligned}
&\sum_{j=1}^{5} I_{rj}\ddot{\theta}_{rj} + \sum_{j=1}^{5} C_{r\theta j}\dot{\theta}_{rj} + \sum_{k=1}^{4} C_{rt\theta k}\left(\dot{\theta}_{rk} - \dot{\theta}_{r(k+1)}\right) + \sum_{j=1}^{5}\sum_{i=1}^{N} C_{rpij}(t)\left(\frac{\partial \Delta_{rpij}}{\partial \theta_{rj}}\right)\cos\beta_b + \sum_{j=1}^{5} K_{r\theta j}\theta_{rj} \\
&\quad + \sum_{k=1}^{4} K_{rt\theta k}\left(\dot{\theta}_{rk} - \dot{\theta}_{r(k+1)}\right) + \sum_{j=1}^{5}\sum_{i=1}^{N} K_{rpij}(t)\Delta_{rpij}\cos\beta_b = 0, \\
&\cdot \sum_{j=1}^{5} m_{rj}\ddot{x}_{rj} + \sum_{j=1}^{5} C_{rxj}\dot{x}_{rj} + \sum_{k=1}^{4} C_{rtxj}\left(\dot{x}_{rk} - \dot{x}_{r(k+1)}\right) - \sum_{j=1}^{5}\sum_{i=1}^{N} C_{rpij}(t)\left(\frac{\partial \Delta_{rpij}}{\partial x_{rj}}\right)\sin\left(\varphi_i + \alpha_{rp}\right)\cos\beta_b \\
&\quad + \sum_{j=1}^{5} K_{rxj}x_{rj} + \sum_{k=1}^{4} K_{rtxj}\left(x_{rk} - x_{r(k+1)}\right) - \sum_{j=1}^{5}\sum_{i=1}^{N} K_{rpij}(t)\Delta_{spij}\sin\left(\varphi_{ij} + \alpha_{rp}\right)\cos\beta_b = 0, \\
&\cdot \sum_{j=1}^{5} m_{rj}\ddot{y}_{rj} + \sum_{j=1}^{5} C_{ryj}\dot{y}_{rj} + \sum_{k=1}^{4} C_{rtyk}\left(\dot{y}_{rk} - \dot{y}_{r(k+1)}\right) + \sum_{j=1}^{5}\sum_{i=1}^{N} C_{rpij}(t)\frac{\partial \Delta_{rpij}}{\partial y_{rj}}\cos\left(\varphi_{ij} + \alpha_{rp}\right)\cos\beta_b \\
&\quad + \sum_{j=1}^{5} K_{ryj}y_{rj} + \sum_{k=1}^{4} K_{rtyk}\left(y_{rk} - y_{r(k+1)}\right) + \sum_{j=1}^{5}\sum_{i=1}^{N} K_{rpij}(t)\Delta_{rpij}\cos\left(\varphi_{ij} + \alpha_{rp}\right)\cos\beta_b = 0, \\
&\cdot \sum_{j=1}^{5} m_{rj}\ddot{z}_{rj} + \sum_{j=1}^{5} C_{rzj}\dot{z}_{rj} + \sum_{k=1}^{4} C_{rtzk}\left(\dot{z}_{rk} - \dot{z}_{r(k+1)}\right) + \sum_{j=1}^{5}\sum_{i=1}^{N} C_{rpij}(t)\frac{\partial \Delta_{rpij}}{\partial z_{rj}}\sin\beta_b + \sum_{j=1}^{5} K_{rzj}z_{rzj} \\
&\quad + \sum_{k=1}^{4} K_{rtzk}\left(z_{rk} - z_{r(k+1)}\right) + \sum_{j=1}^{5}\sum_{i=1}^{N} K_{rpij}(t)\Delta_{rpij}\sin\beta_b = 0.
\end{aligned}
\tag{4}
$$

Kinetic equations of the 1st stage planet gear (ith)

$$\begin{aligned}
&\sum_{j=1}^{5}\sum_{i=1}^{5} I_{pij}\ddot{\theta}_{pij} - \sum_{i=1}^{5}\sum_{k=1}^{4} C_{ptik}\left(\dot{\theta}_{pik} - \dot{\theta}_{pi(k+1)}\right) + \sum_{j=1}^{5}\sum_{i=1}^{N} C_{spij}(t)\frac{\partial \Delta_{spij}}{\partial \theta_{pij}}\cos\beta_b - \sum_{j=1}^{5}\sum_{i=1}^{N} C_{rpij}(t)\frac{\partial \Delta_{rpij}}{\partial \theta_{pij}}\cos\beta_b \\
&- \sum_{i=1}^{5}\sum_{k=1}^{4} K_{ptik}\left(\theta_{pik} - \theta_{pi(k+1)}\right) - \sum_{j=1}^{5}\sum_{i=1}^{N} K_{spij}(t)\Delta_{spij}\cos\beta_b - \sum_{j=1}^{5}\sum_{i=1}^{N} K_{rpij}(t)\Delta_{rpij}\cos\beta_b = 0, \\
&\cdot\sum_{j=1}^{5} m_{pij}\ddot{u}_{pij} + \sum_{j=1}^{5} C_{piju}\dot{u}_{pij} - \sum_{j=1}^{5} C_{piju}(t)\frac{\partial \delta_{piju}}{\partial u_{pij}} + \sum_{k=1}^{4} K_{ptiku}\left(\dot{u}_{pik} - \dot{u}_{pi(k+1)}\right) - \sum_{j=1}^{5} C_{spij}(t)\frac{\partial \Delta_{spij}}{\partial u_{pij}}\sin\alpha_{sp}\cos\beta_b \\
&+ \sum_{j=1}^{5} C_{rpij}(t)\frac{\partial \Delta_{rpij}}{\partial u_{pij}}\sin\alpha_{rp}\cos\beta_b + \sum_{j=1}^{5} K_{piju}u_{pij} - \sum_{j=1}^{5} K_{piju}(t)\delta_{piju} + \sum_{k=1}^{4} K_{ptiku}\left(u_{pik} - u_{pi(k+1)}\right) \\
&- \sum_{j=1}^{5} K_{spij}(t)\Delta_{spij}\sin\alpha_{sp}\cos\beta_b + \sum_{j=1}^{5} K_{rpij}(t)\Delta_{rpi}\sin\alpha_{rp}\cos\beta_b = 0, \\
&\cdot\sum_{j=1}^{5} m_{pij}\ddot{v}_{pij} + \sum_{j=1}^{5} C_{pijv}\dot{v}_{pij} - \sum_{j=1}^{5} C_{pijv}(t)\frac{\partial \delta_{pijv}}{\partial v_{pij}} + \sum_{k=1}^{4} C_{ptikv}\left(\dot{v}_{pik} - \dot{v}_{pi(k+1)}\right) + \sum_{j=1}^{5} C_{spij}(t)\frac{\partial \Delta_{spij}}{\partial v_{pij}}\cos\alpha_{sp}\cos\beta_b \\
&- \sum_{j=1}^{5} C_{rpij}(t)\frac{\partial \Delta_{rpij}}{\partial v_{pij}}\cos\alpha_{rp}\cos\beta_b + \sum_{j=1}^{5} K_{pijv}v_{pij} - \sum_{j=1}^{5} K_{pijv}(t)\delta_{pijv} + \sum_{k=1}^{4} K_{ptikv}\left(v_{pik} - v_{pi(k+1)}\right) \\
&+ \sum_{j=1}^{5} K_{spij}(t)\Delta_{spij}\cos\alpha_{sp}\cos\beta_b - \sum_{j=1}^{5} K_{rpij}(t)\Delta_{rpij}\cos\alpha_{rp}\cos\beta_b = 0, \\
&\cdot\sum_{j=1}^{5} m_{pij}\ddot{w}_{pij} + \sum_{j=1}^{5} C_{pijw}\dot{w}_{pij} + \sum_{j=1}^{5} C_{pijw}(t)\frac{\partial \delta_{pijw}}{\partial w_{pij}} + \sum_{k=1}^{4} C_{ptikw}\left(\dot{w}_{pik} - \dot{w}_{pi(k+1)}\right) - \sum_{j=1}^{5} C_{spij}(t)\frac{\partial \Delta_{spij}}{\partial w_{pij}}\sin\beta_b \\
&- \sum_{j=1}^{5} C_{rpij}(t)\frac{\partial \Delta_{rpij}}{\partial w_{pij}}\sin\beta_b + \sum_{j=1}^{5} K_{pijw}w_{pij} + \sum_{j=1}^{5} K_{pijw}(t)\delta_{pijw} - \sum_{j=1}^{5} K_{spij}(t)\Delta_{spij}\sin\beta_b + \sum_{k=1}^{4} K_{ptikw}\left(w_{pik} - w_{pi(k+1)}\right) \\
&- \sum_{j=1}^{5} K_{rpij}(t)\Delta_{rpij}\sin\beta_b = 0.
\end{aligned} \tag{5}$$

Kinetic equations of the 1st stage carrier

$$\begin{aligned}
&\sum_{j=1}^{5} I_{cj}\ddot{\theta}_{cj} + \sum_{j=1}^{5}\sum_{i=1}^{N} C_{pijv}(t)\frac{\partial \delta_{pijv}}{\partial \theta_{cj}} + + \sum_{j=1}^{5}\sum_{i=1}^{N} K_{pijv}(t)\delta_{pijv} + \sum_{j=1}^{5}\sum_{i=1}^{N} C_{spij}(t)\frac{\partial \delta_{pijv}}{\partial \theta_{cj}} + \sum_{j=1}^{5}\sum_{i=1}^{N} C_{rpij}(t)\frac{\partial \Delta_{rpij}}{\partial \theta_{cj}} \\
&+ \sum_{k=1}^{4} C_{ctk}\left(\dot{\theta}_{ck} - \dot{\theta}_{c(k+1)}\right) + \sum_{j=1}^{5}\sum_{i=1}^{N} K_{spij}(t)\Delta_{spij} + \sum_{j=1}^{5}\sum_{i=1}^{N} K_{rpij}(t)\Delta_{rpij} + \sum_{k=1}^{4} K_{ctk}\left(\theta_{ck} - \theta_{c(k+1)}\right) = T_{in},
\end{aligned}$$

Table 2: Stiffnesses of the HPTS.

Subject	Kx (N/m)	Ky (N/m)	Kz (N/m)	Kθ (N/rad)
Ring support	3e11	3e11	1e11	5e11
Sun bearing	2.6e9	2.66e9	3.5e8	—
Planet bearing	3.0e9	3.0e9	4.6e8	—
Carrier support	4.8e10	4.8e10	8.4e9	—
Sun-planet gear meshing (N/m)		8.63e9		
Ring-planet gear meshing (N/m)		10.9e9		

$$
\begin{aligned}
&\cdot \sum_{j=1}^{5} m_{cj}\ddot{x}_{cj} + \sum_{j=1}^{5} C_{cxj}\dot{x}_{cj} + \sum_{j=1}^{5}\sum_{i=1}^{N} C_{piju}(t)\frac{\partial \delta_{piju}}{\partial x_{cj}}\cos\varphi_i - \sum_{j=1}^{5}\sum_{i=1}^{N} C_{pijv}(t)\frac{\partial \delta_{pijv}}{\partial x_{cj}}\sin\varphi_i + \sum_{k=1}^{4} C_{ctxk}\left(\dot{x}_{ck} - \dot{x}_{c(k+1)}\right) \\
&+ \sum_{j=1}^{5} K_{cxj}x_{cj} + \sum_{i=1}^{N} K_{piju}(t)\delta_{piju}\cos\varphi_i - \sum_{i=1}^{N} K_{pijv}(t)\delta_{pijv}\sin\varphi_i + \sum_{k=1}^{4} K_{ctxk}\left(x_{ck} - x_{c(k+1)}\right) = 0, \\
&\cdot \sum_{j=1}^{5} m_{cj}\ddot{y}_{cj} + \sum_{j=1}^{5} C_{cyj}\dot{y}_{cj} + \sum_{j=1}^{5}\sum_{i=1}^{N} C_{piju}(t)\frac{\partial \delta_{piju}}{\partial y_{cj}}\sin\varphi_i + \sum_{j=1}^{5}\sum_{i=1}^{N} C_{pijv}(t)\frac{\partial \delta_{pijv}}{\partial y_{cj}}\cos\varphi_i + \sum_{k=1}^{4} C_{ctyk}\left(\dot{y}_{ck} - \dot{y}_{c(k+1)}\right) \\
&+ \sum_{j=1}^{5} K_{cyj}y_{cj} + \sum_{j=1}^{5}\sum_{i=1}^{N} K_{piju}(t)\delta_{piju}\sin\varphi_i + \sum_{j=1}^{5}\sum_{i=1}^{N} K_{pijv}(t)\delta_{pijv}\cos\varphi_i + \sum_{k=1}^{4} K_{ctyk}\left(y_{ck} - y_{c(k+1)}\right) = 0, \\
&\cdot \sum_{j=1}^{5} m_{cj}\ddot{z}_{cj} + \sum_{j=1}^{5} C_{czj}\dot{z}_{cj} + \sum_{k=1}^{4} C_{ctzk}\left(\dot{z}_{ck} - \dot{z}_{c(k+1)}\right) + \sum_{j=1}^{5}\sum_{i=1}^{N} C_{pijw}(t)\left(\dot{z}_{cj} - \dot{w}_{pij}\right) + \sum_{j=1}^{5} K_{czj}z_{cj} \\
&+ \sum_{k=1}^{4} k_{ctzk}\left(z_{ck} - z_{c(k+1)}\right) + \sum_{j=1}^{5}\sum_{i=1}^{N} K_{pijw}(t)\left(z_{cj} - w_{pij}\right) = 0.
\end{aligned}
\tag{6}
$$

The equations of motion for the above transmission components are sorted out, and the dynamic equation matrix form of the HPTS considering the influence of the installation shaft error is

$$[M][\ddot{q}] + [C][\dot{q}] + [K][q] = [Q], \tag{7}$$

where M, C, K, and Q are system mass matrix, damping matrix, stiffness matrix, and external load matrix, respectively, and $\ddot{q}$, $\dot{q}$, and q are system vibration acceleration matrix, vibration velocity matrix, and vibration displacement matrix, respectively. The system has 160 DOFs of which the planet carrier, sun gear, and ring gear have 60 DOFs, respectively, and the 5 evenly distributed planetary gears have 100 DOFs.

3. Dynamic Responses of the HPTS

The input torque of the system is 4.88e6 Nm, and the load torque is 1.18e6 Nm. The mesh stiffnesses of gear pairs are calculated from the Romax according to the ISO6336-2008 standard, and the Fourier series was used to calculate the stiffness excitation harmonics. The stiffnesses of the HPTS are listed in Table 2.

Figures 5 and 6 show the vibration acceleration responses and FFT transformations of the central position for the sun gear and ring gear of the HPTS under the positive 0.13 mm IEOS of the 1st planet gear.

As is shown in Figure 5, the maximum vibration acceleration for the FFT amplitude of the sun gear under the positive 0.13 mm IEOS of the 1st planet gear is horizontal direction 3.66 m/s2, and the minimum vibration acceleration for the FFT amplitude is axial direction 1.84 m/s2. Compared with no IEOS condition, the horizontal vibration acceleration amplitude increased by 8.3%, and the axial vibration acceleration amplitude increased by 8.2%.

As is shown in Figure 6, the maximum vibration acceleration for the FFT amplitude of the ring gear is vertical direction 2.38 m/s2, and the minimum axial vibration acceleration for the FFT amplitude is 1.07 m/s2 considering the positive 0.13 mm IEOS of the 1st planet gear. Compared with no IEOS condition, the vibration acceleration amplitude for the vertical direction of the ring gear increased by 11.2%, and the vibration acceleration amplitude for the axial direction increased by 11.5%.

In general, the vibration accelerations for the FFT responses of the sun gear and ring gear show three times the gear meshing frequency of the system. Due to the IEOS of the 1st planet gear, the FFT amplitudes in all directions for vibration acceleration response of transmission components are increased to a certain extent at the gear meshing

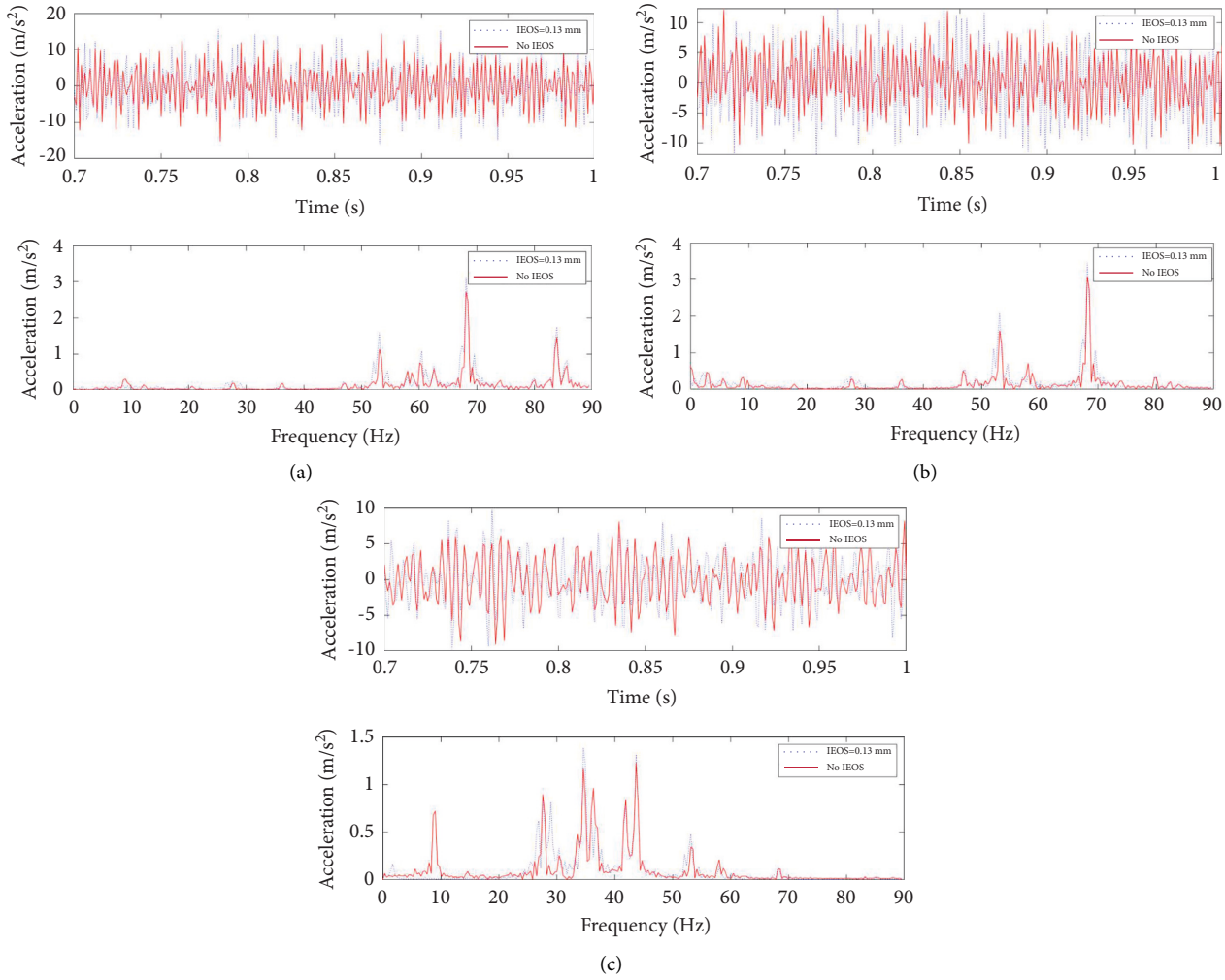

Figure 5: Vibration acceleration responses for sun gear under the IEOS of the 1st planet gear. (a) Horizontal direction. (b) Vertical direction. (c) Axial direction.

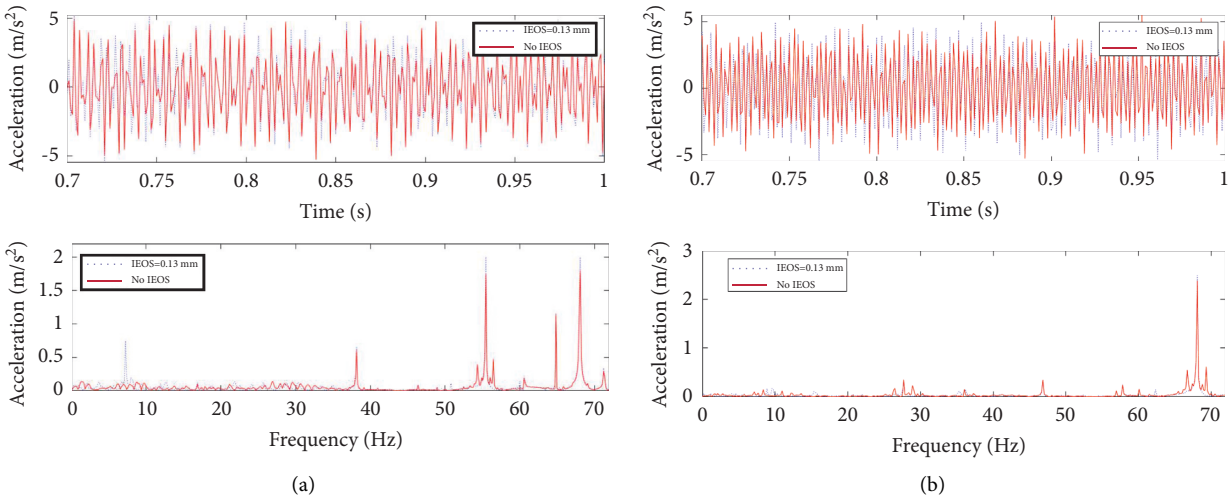

Figure 6: Continued.

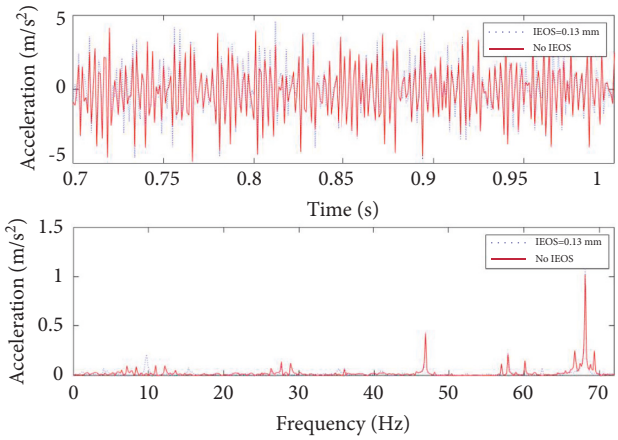

(c)

Figure 6: Vibration acceleration responses ring gear under the IEOS of the 1st planet gear. (a) Horizontal direction. (b) Vertical direction. (c) Axial direction.

frequency position. Compared with no IEOS of the 1st planet gear, the maximum magnitude increase of the vibration acceleration for the FFT amplitude under the IEOS condition for the 1st planet gear is the axial direction of the ring gear.

The overall trend and characteristics for the influence of the planetary gear IEOS on the responses of the gear pair meshing force are consistent with the literature [9, 12]. The influence situation and characteristics of the IEOS of the 1st planet gear on the vibration accelerations for the transmission components of the system are consistent with the literature [13]. The results show that the IEOS of the 1st planet gear has a significant influence on the vibration response characteristics of the HPTS.

4. Conclusions

A lumped parameter dynamic model of a 5-slice type HPTS is established considering the factors of the IEOS for the 1st planet gear and the time-varying meshing characteristics of gear pairs. The characteristics of the vibration influence for the HPTS under the IEOS are analyzed. The main conclusions are as follows:

(1) Compared with no IEOS condition, the FFT amplitudes for the horizontal vibration acceleration of the sun gear increased 8.3% and the axial vibration acceleration of the ring gear increased 11.5% considering the positive 0.13 mm IEOS for the 1st planet gear, respectively.

(2) The vibration accelerations for the FFT responses of the sun gear and ring gear show three times the gear meshing frequency of the system considering a positive 0.13 mm IEOS for the 1st planet gear. The maximum magnitude increase of the vibration acceleration for the FFT amplitude under a positive 0.13 mm IEOS for the 1st planet gear is the axial direction of the ring gear. The results show that the IEOS of the 1st planet gear has a significant influence on the vibration response characteristics of the HPTS.

(3) In the modeling of a 5-slice type HPTS considering the factors of the IEOS for the 1st planet gear, the influence of the time-varying support stiffness for the bearings on the system vibration needs to be taken into account. The IEOS needs to be thoroughly introduced into the HPTS to simulate actual operating conditions.

Data Availability

The data used to support the findings of this study are included within the article.

Conflicts of Interest

The authors declare that they have no conflicts of interest.

Acknowledgments

This work was supported by the Major Science and Technology Projects in Henan Province (Grant no. 191110210100), the Key Scientific and Technological Projects in Henan Province (Grant nos. 212102210361 and 202102210272), the National Natural Science Foundation of China (Grant no. 52075500), the Training Program for Young Backbone Teachers in Colleges and Universities of Henan Province (Grant no. 2019GGJS130), and the Zhengzhou University of Light Technology Doctoral Research Initiation Fund (Grant no. 2017BSJJ016). The Applied Research Plan for Key Scientific Research Projects in Colleges and Universities (Grant no. 19A460032) is gratefully acknowledged.

References

[1] J. Helsen, F. Vanhollebeke, F. De Coninck, D. Vandepitte, and W. Desmet, "Insights in wind turbine drive train dynamics gathered by validating advanced models on a newly developed

13.2MW dynamically controlled test-rig," *Mechatronics*, vol. 21, no. 4, pp. 737–752, 2011.

[2] J. Helsen, F. Vanhollebeke, B. Marrant, D. Vandepitte, and W. Desmet, "Multibody modelling of varying complexity for modal behaviour analysis of wind turbine gearboxes," *Renewable Energy*, vol. 36, no. 11, pp. 3098–3113, 2011.

[3] M. Zhao and J. C. Ji, "Nonlinear torsional vibrations of a wind turbine gearbox," *Applied Mathematical Modelling*, vol. 39, no. 16, pp. 4928–4950, 2015.

[4] X. Gu and P. Velex, "A dynamic model to study the influence of planet position errors in planetary gears," *Journal of Sound and Vibration*, vol. 331, no. 20, pp. 4554–4574, 2012.

[5] X. Gu and P. Velex, "On the dynamic simulation of eccentricity errors in planetary gears," *Mechanism and Machine Theory*, vol. 61, pp. 14–29, 2013.

[6] C. Wang and R. G. Parker, "Modal properties and parametrically excited vibrations of spinning epicyclic/planetary gears with a deformable ring," *Journal of Sound and Vibration*, vol. 494, Article ID 115828, 2021.

[7] A. Tatar, C. W. Schwingshackl, and M. I. Friswell, "Dynamic behaviour of three-dimensional planetary geared rotor systems," *Mechanism and Machine Theory*, vol. 134, pp. 39–56, 2019.

[8] Z. Shen, B. Qiao, L. Yang, W. Luo, R. Yan, and X. Chen, "Dynamic modeling of planetary gear set with tooth surface wear," *Procedia Manufacturing*, vol. 49, pp. 49–54, 2020.

[9] J. Liu, R. Pang, S. Ding, and X. Li, "Vibration analysis of a planetary gear with the flexible ring and planet bearing fault," *Measurement*, vol. 165, no. 4, Article ID 108100, 2020.

[10] A. Mbarek, A. Hammami, A. Fernandez Del Rincon, F. Chaari, F. Viadero Rueda, and M. Haddar, "Effect of load and meshing stiffness variation on modal properties of planetary gear," *Applied Acoustics*, vol. 147, pp. 32–43, 2019.

[11] B. Zghal, O. Graja, K. Dziedziech et al., "A new modeling of planetary gear set to predict modulation phenomenon," *Mechanical Systems and Signal Processing*, vol. 127, no. 15, pp. 234–261, 2019.

[12] J. T. Kahnamouei and J. Yang, "Development and verification of a computationally efficient stochastically linearized planetary gear train model with ring elasticity," *Mechanism and Machine Theory*, vol. 155, Article ID 104061, 2021.

[13] J. Park, M. Hamadache, J. M. Ha, Y. Kim, K. Na, and B. D. Youn, "A positive energy residual (PER) based planetary gear fault detection method under variable speed conditions," *Mechanical Systems and Signal Processing*, vol. 117, pp. 347–360, 2019.

[14] S. Li and A. Kahraman, "A scuffing model for spur gear contacts," *Mechanism and Machine Theory*, vol. 156, no. 2, Article ID 104161, 2021.

[15] M. N. Anandika, A. Kahraman, and D. Talbot, "An experimental investigation of the impact of random spacing errors on the dynamic transmission error of spur gear pairs," in *Proceedings of the 2019 International Design Engineering Technical Conferences and Computers and Information in Engineering Conference*, Anaheim, CA, USA, August 2019.

[16] G. Liu, J. Hong, and R. G. Parker, "Influence of simultaneous time-varying bearing and tooth mesh stiffness fluctuations on spur gear pair vibration," *Nonlinear Dynamics*, vol. 97, no. 2, pp. 1403–1424, 2019.

[17] T. M. Ericson and R. G. Parker, "Experimental measurement and finite element simulation of elastic-body vibration in planetary gears," *Mechanism and Machine Theory*, vol. 160, no. 4, Article ID 104264, 2021.

[18] F. Ren, J. Ji, G. Luo et al., "Investigation of dynamic load sharing behavior for herringbone planetary gears considering multicoupling manufacturing errors," *Shock and Vibration*, vol. 2021, Article ID 5511817, 15 pages, 2021.

[19] Y. Liu, D. Zhen, H. Zhang, H. Zhang, Z. Shi, and F. Gu, "Vibration response of the planetary gears with a float sun gear and influences of the dynamic parameters," *Shock and Vibration*, vol. 2020, no. 1, 17 pages, Article ID 8886066, 2020.

[20] K. Feng, K. Wang, Q. Ni, M. J. Zuo, and D. Wei, "A phase angle based diagnostic scheme to planetary gear faults diagnostics under non-stationary operational conditions," *Journal of Sound and Vibration*, vol. 408, pp. 190–209, 2017.

[21] K. Feng, K. Wang, M. Zhang, Q. Ni, and M. J. Zuo, "A diagnostic signal selection scheme for planetary gearbox vibration monitoring under non-stationary operational conditions," *Measurement Science and Technology*, vol. 28, no. 3, Article ID 035003, 2017.